SCIENCE CHINA Materials

ARTICLES

mater.scichina.com link.springer.com

Published online 26 April 2017 | doi: 10.1007/s40843-017-9033-5
Sci China Mater 2017, 60(5): 427–437

Hollow and hierarchical $Na_2Li_2Ti_6O_{14}$ microspheres with high electrochemical performance as anode material for lithium-ion battery

Shan-Shan Fan[1], Hua Zhong[1], Hai-Tao Yu[1], Ming Lou[1], Ying Xie[1*] and Yan-Rong Zhu[2*]

ABSTRACT **Relying on a solvent thermal method, spherical $Na_2Li_2Ti_6O_{14}$ was synthesized. All samples prepared by this method are hollow and hierarchical structures with the size of about 2–3 μm, which are assembled by many primary nanoparticles (~300 nm). Particle morphology analysis shows that with the increase of temperature, the porosity increases and the hollow structure becomes more obvious. $Na_2Li_2Ti_6O_{14}$ obtained at 800°C exhibits the best electrochemical performance among all samples. Charge-discharge results show that $Na_2Li_2Ti_6O_{14}$ prepared at 800°C can delivers a reversible capacity of 220.1, 181.7, 161.6, 144.2, 118.1 and 97.2 mA h g^{-1} at 50, 140, 280, 560, 1400, 2800 mA g^{-1}. However, $Na_2Li_2Ti_6O_{14}$-bulk only delivers a reversible capacity of 187, 125.3, 108.3, 88.7, 69.2 and 54.8 mA h g^{-1} at the same current densities. The high electrochemical performances of the as-prepared materials can be attributed to the distinctive hollow and hierarchical spheres, which could effectively reduce the diffusion distance of Li ions, increase the contact area between electrodes and electrolyte, and buffer the volume changes during Li ion intercalation/deintercalation processes.**

Keywords: $Na_2Li_2Ti_6O_{14}$, hollow structure, anode material, electrochemical performance, lithium ion battery

INTRODUCTION

In the past two decades, lithium ion batteries (LIBs) have been widely used as an important power source for portable electronic products, electric vehicles, and large-scale grid energy storage because of their high energy density, long cycle life, and environmental benignity [1–4]. Although carbon-based anodes were successfully applied in the first generation LIBs in the very beginning, they have been replaced by other anode materials nowadays owning to their limited capacity and efficiency, short cycling life, and safety hazard [5]. A promising alternative is the Ti-based anode materials. Spinel lithium titanium oxide ($Li_4Ti_5O_{12}$) with a flat plateau at about 1.55 V (*vs.* Li/Li^+) is one of the most popular anode materials for Li-ion batteries [6], and it can be discharged down to 0 V (*vs.* Li/Li^+) without causing any structural degradations (zero-strain insertion material) [7]. Similarly, mixed alkali titanium oxides, $M_xLi_2Ti_6O_{14}$ (M = Ba, Sr, Na_2), were also proposed recently [8–10]. By introducing alkali derivatives into titanium dioxides, the potential of the anode materials can be lowered [11]. It was reported that the potential of $SrLi_2Ti_6O_{14}$ with respect to lithium metal electrode is 1.35 V [12] , whereas the value for $Na_2Li_2Ti_6O_{14}$ (NLTO) is about 1.28 V [13]. For a full-battery, the lower potential of an anode means a larger open cell voltage (OCV) and is thus helpful for the increase of mass energy density and volume energy density. The excellent thermodynamic stabilities of titanates also lead to a good reversibility and cycling stability for the materials, which is crucial for LIB applications.

However, the oxidation state of titanium (Ti^{4+}) in TiO_2 and $Li_4Ti_5O_{12}$ will cause the separation of the valence and conduction bands, giving rise to large band gaps [14–17]. It was also reported that $M_xLi_2Ti_6O_{14}$ anode materials do have poor electronic conductivities and low lithium-ion diffusion coefficients. This intrinsic flaw in titanates will result in poor rate capability. To solve this problem, strategies including carbon coating [18], metal ions doping [19–21],

[1] Key Laboratory of Functional Inorganic Material Chemistry, Ministry of Education, School of Chemistry and Materials Science, Heilongjiang University, Harbin 150080, China
[2] School of Chemistry and Chemical Engineering, Anhui University of Technology, Maanshan 243002, China
* Corresponding authors (emails: xieying@hlju.edu.cn (Xie Y); zhuyrong@ahut.edu.cn (Zhu YR))

and conducting layer coating [22,23] were applied. Alternatively, the structural changes and the morphology of the electrode materials can also significantly affect their electrochemical properties [24,25]. It was demonstrated that the void space in hollow micro-particles can provide additional sites for lithium storage and is beneficial for the improvement of the reversible capacity [26]. The surface area of the hollow micro-particles is usually much larger than that of solid materials, leading to a much better contact and infiltration between the electrode and electrolyte [27]. Therefore, lithium diffusion between the electrode and electrolyte would be much easier, and the interfacial impedance and rate capability are thus expected to be improved [28,29]. Furthermore, thanks to the hollow structures, the electrode materials are more tolerant to the stresses and strains induced by repeated insertion and extraction of lithium. The tolerance of the volume is of great importance for the improvement of the cycling performance [30].

Although previous investigations have suggested that the hollow structures are rather helpful for improving the electrochemical properties of the electrode materials, to the best of our knowledge, the synthesis of $Na_2Li_2Ti_6O_{14}$ in the literatures is still mainly based on the solid states reactions at present [31,32] and the impact of the morphology on the electrochemical performance of $Na_2Li_2Ti_6O_{14}$ is still unclear. And it is also known that commercial $Li_4Ti_5O_{12}$ is usually discharged to 1.0 V, and high safety can be achieved at a cost of some performance redundancy. However, to improve simultaneously the electrochemical performance and safety of the anode materials, especially at extremely low potential condition, the questions and answers concerning on whether the structural integrity of the NLTO materials can be maintained, and whether they can exhibit satisfactory electrochemical performance or not become scientifically important and deserve our further considerations.

With these motivations in mind, in this work, we demonstrated that hollow and hierarchical $Na_2Li_2Ti_6O_{14}$ with high electrochemical performances can be prepared, and the electrochemical performance discharged to 0.0 V was also evaluated. The same strategy can also be applied to synthesize relevant doping materials, which opens a way for the optimization of this anode material in the future.

EXPERIMENTAL SECTION

Preparation of the samples

Traditional solid-state synthesis method is difficult to control the structures and morphologies of the electrode material [20,31], which will lead to unsatisfactory electrochemical performance. To improve the electrochemical properties, a solvothermal synthesis method was thus introduced in the present investigation. First, 16 mmol lithium acetate and 16 mmol sodium acetate were dissolved in 30 mL ethanol at room temperature under vigorous stirring, and then equivalent molar tetrabutyl titanate was added to the solution dropwise. After stirring for 30 min, the homogenized solution was transferred to a 100-mL Teflon-lined stainless steel autoclave, and 0.72 g NH_4HCO_3 was also added into the reactor, which was then sealed and heated in an electric oven at 180°C for 12 h. After being cooled down, the white product was collected by centrifugation and washed with ethanol for several times, followed by a drying procedure in an oven at 70°C for 6 h. Because calcination temperature may have an effect on the structure and morphology, heating was performed at a range of 500–900°C for 10 h in air.

To identify the effect of morphology on the electrochemical properties, bulk $Na_2Li_2Ti_6O_{14}$ sample (NLTO-bulk) was synthesized from a classic solid-state reaction as reported in literature [31]. The annealing process was kept at 800°C for 10 h in air. For convenience, hollow hierarchical microspheres at different temperatures and bulk materials were labeled as NLTO-500, NLTO-600, NLTO-700, NLTO-800, NLTO-900 and NLTO-bulk, respectively.

Characterizations and performance tests

X-ray diffraction (XRD) patterns were obtained by using Bruker D8. Scanning electron microscopy (SEM) micrographs were taken by using a Hitachi S-4800 instrument operating at 15 kV. Transmission electron microscopy (TEM) and high-resolution TEM (HRTEM) images of the samples were recorded by a JEOL 2100 microscope with an accelerating voltage of 200 kV.

The electrochemical performance of $Na_2Li_2Ti_6O_{14}$ was tested in a half-cell, in which metal lithium was adopted as a counter electrode. The working electrode materials were composed of 80 wt.% $Na_2Li_2Ti_6O_{14}$ (160 mg), 10 wt.% carbon black (20 mg), and 10 wt.% polyinylidene fluorides (PVDF) (20 mg). These materials were uniformly mixed in *N*-methyl-2-pyrrolidinone (NMP), and then the formed homogeneous slurry was applied to a copper-foil current collector. The electrode was dried at 110°C in a vacuum oven for 12 h to remove excess solvent, and then pressed at 3 MPa. The mass loadings for NTLO-700, NTLO-800 and NTLO-bulk electrodes were 0.93, 0.86 and 0.80 mg, respectively. Celgard 2400 films were used as separators, and the electrolyte was a 1 mol L^{-1} $LiPF_6$

solution dissolved in a 1:1:1 (*v*/*v*/*v*) mixture of ethylene carbonate (EC), diethyl carbonate (DEC), and dimethyl carbonate (DMC). Battery assembly was carried out in a recirculating Ar glove-box, where the moisture and oxygen contents were below 1 ppm. Charge-discharge cycles of the half-cells were evaluated between 0 and 3 V (*vs.* Li^+/Li) at room temperature by using a LAND CT2001A system under different rates. Electrochemical impedance spectroscopy (EIS) was conducted by using a Princeton P4000 electrochemical workstation over a frequency range from 0.01 Hz to 100 kHz at a potentiostatic signal amplitude of 5 mV. Cyclic voltammetry (CV) test was carried out on a CHI 1000C electrochemical workstation with a voltage between 0 and 3 V at a scanning rate of 0.1 mV s^{-1}.

RESULTS AND DISCUSSION

The XRD patterns of $Na_2Li_2Ti_6O_{14}$ obtained from 500 to 900°C are shown in Fig. 1. It can be clearly observed that well-crystalline $Na_2Li_2Ti_6O_{14}$ is rather difficult to be detected below 500°C. However, it was confirmed that the main diffraction peaks of other samples calcined from 600 to 800°C were well matched with the standard powder diffraction file (JCPDS card No. 52-0690) and the results of previous reports [31,32].

Furthermore, no impurity such as TiO_2 and $Li_4Ti_5O_{12}$ can be observed in the figure. It should be noticed that in comparison to the low temperature sample (600°C), the diffraction peaks of $Na_2Li_2Ti_6O_{14}$ obtained at 700 and 800°C (Fig. 1e, f) are much stronger and sharper, indicating significant improvement of the crystalline degree. With continuous

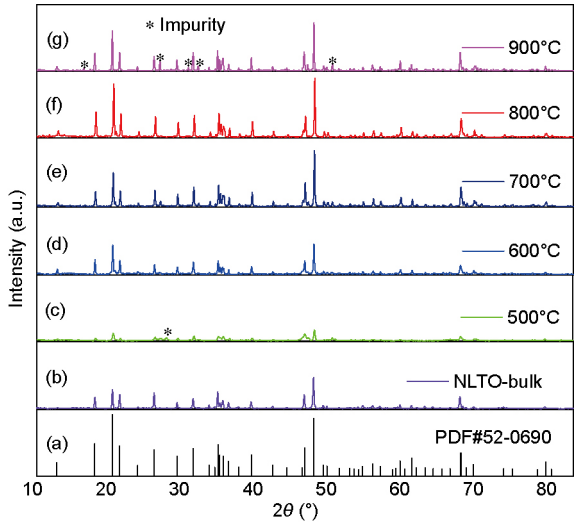

Figure 1 XRD patterns of $Na_2Li_2Ti_6O_{14}$ power prepared at different temperatures. (a) Standard PDF#52-0690, (b) NLTO-bulk, NLTO obtained at (c) 500°C, (d) 600°C, (e) 700°C, (f) 800°C and (g) 900°C.

increase of temperature, an impure phase corresponding to a $C_{2/m}$ symmetry (JCPDS card No. 53-0387) appears at 900°C. It can be further identified that this impure phase is $Na_{0.69}Li_{0.4}Ti_{3.73}O_8$ ($Na_{0.78}Li_{1.20}O_2$ deficiency). In comparison to the samples obtained at the same temperature by a solid state reaction [31], the size of our sample is much smaller, making them more easily to be affected by the temperature. As a result, the evaporation of Na_2O and Li_2O in NLTO-900 samples should be more severe, leading to the appearance of impurities. The results show that higher calcination temperature is not always beneficial to the structural integrity of the samples.

To reveal the structural details, XRD Rietveld refinement of the $Na_2Li_2Ti_6O_{14}$ samples obtained at different synthetic conditions was performed and the results were shown in Table 1 and Fig. 2. It was confirmed that Na and Li are located at 8h and 8a sites, while Ti occupies 8f and 16m sites (Fig. 2). Moreover, the refinement data indicate that the lattice parameters of *a*, *b* and *c* for all samples are almost identical. For example, the lattice parameters of NLTO-800 are a = 16.4906, b = 5.7434, and c = 11.2258 Å, in good agreement with previous reports [20,21,31]. Because of the nearly identical lattice constants, the effect of structural and morphology changes on the electrochemical performance can be identified.

The surface morphologies of $Na_2Li_2Ti_6O_{14}$ calcined at different temperatures are shown in Fig. 3. As can be seen from the images, all samples prepared by the solvent thermal method are spherical structures with a size of about 2–3 μm, which are assembled by many primary nanoparticles (~300 nm). It can be clearly seen from Fig. 3a, b that the sample calcined at 600°C is poorly crystalline, and the contact among the nanoparticles is more compact. As the temperature increases, the porosity increases and the hollow structure becomes obvious. At 700 and 800°C, the obtained samples possess uniform hollow structures. Furthermore, our experiments also confirmed that the materials were unable to form any special morphology without adding NH_4HCO_3 during the synthesis process, as shown in Fig. S2 of the Supplementary information. Therefore, the origin of the hollow structures can be attributed to the

Table 1 Lattice constants calculated from XRD Rietveld refinement for different samples

	NLTO-bulk	NLTO-600	NLTO-700	NLTO-800
a (Å)	16.5024	16.4896	16.4736	16.4906
b (Å)	5.7516	5.7431	5.7383	5.7434
c (Å)	11.2309	11.2268	11.2172	11.2258

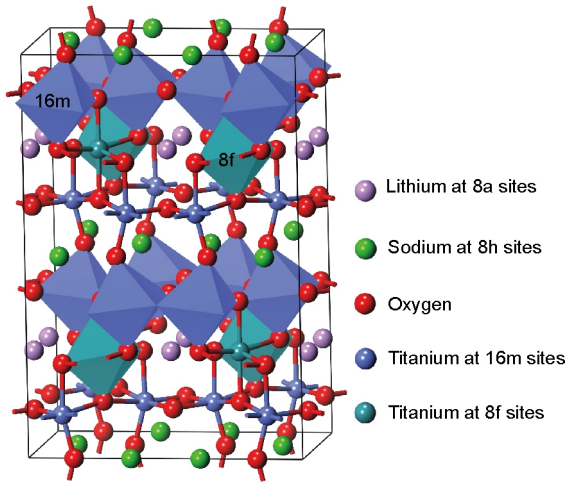

Figure 2 Crystal structure of $Na_2Li_2Ti_6O_{14}$ compounds.

decomposition of ammonium bicarbonate during the synthesis process, in which the generation of gases may act as a soft template to induce the growth of the materials to form specific morphologies. While the subsequence calcinations at different temperature will affect the pore size and assemble state of the nanoparticles, leading to different structures and morphologies. It can be expected that the changes of the morphologies will result in different electrochemical performances.

TEM images for NLTO-800 sample are shown in Fig. 4. As can be seen from the figure, all the microspheres are hollow structures with a diameter of about 2 μm. The wall thickness of the microspheres assembled by a series of nanoparticles is around 400 nm. This observation is consistent with the SEM results. Because of the hollow structures and the primary nanoparticles, the diffusion kinetics of lithium insertion/extraction of the as-prepared samples should be significantly improved, leading to lower polarizations and overpotentials. Furthermore, the HRTEM also clearly shows that the lattice fringe distances of the sample (3.30 Å) corresponds to the fingerprint of {402} planes, which is coincident with the XRD results and previous reports [33].

Elemental distribution of the electrode materials is important and usually related to their electrochemical properties [34]. To visualize the distributions of Na, Ti and O elements, energy-dispersive X-ray spectroscopy (EDS) mapping for NLTO-800 sample was performed. Fig. 5 shows that Na, Ti and O elements are distributed evenly at the whole region, and the atomic ratio of Na and Ti is calculated to be 0.43, which is close to the stoichiometry of $Na_2Li_2Ti_6O_{14}$.

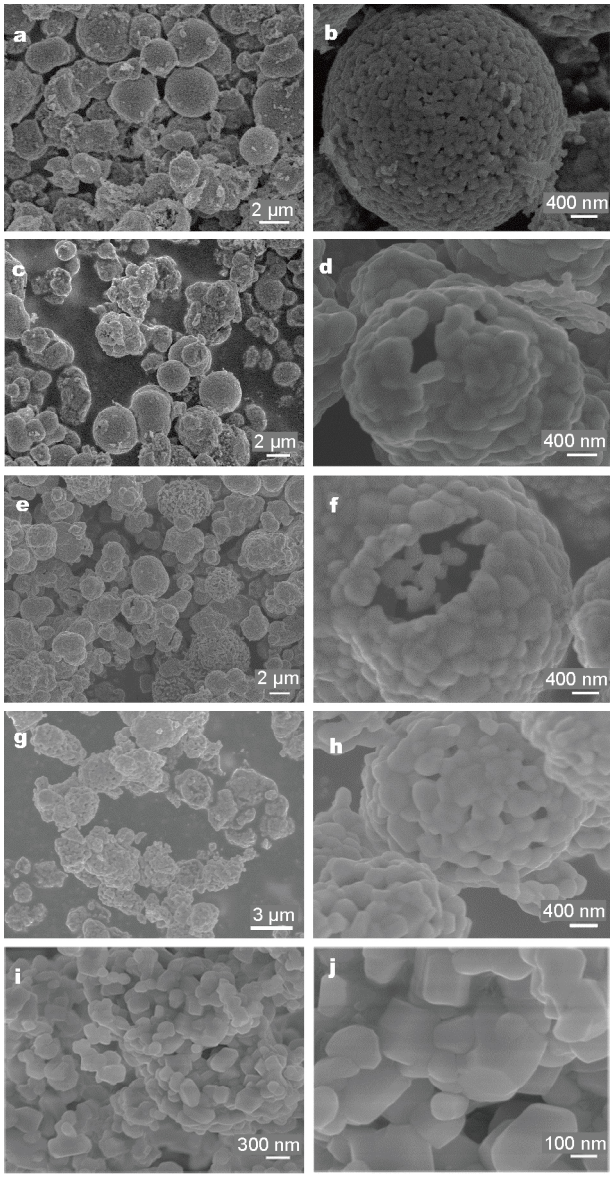

Figure 3 SEM images of $Na_2Li_2Ti_6O_{14}$ powder prepared at different temperatures. (a, b) 600°C, (c, d) 700°C, (e, f) 800°C, (g, h) 900°C and (i, j) NLTO-bulk.

The CV curves of different samples obtained at a scan rate of 0.1 mV s^{-1} between 0.0 and 3.0 V are shown in Fig. 6. It was demonstrated that only one pair of redox peaks corresponding to the extraction/insertion of lithium from/into the lattice for each cycle appears. The cathodic/anodic peaks are located at about 1.20/1.37, 1.17/1.39 and 1.18/1.35 V for NLTO-700, NLTO-800 and NLTO-bulk, respectively, which can be attributed to the oxidation/reduction of Ti^{3+}/Ti^{4+} couple [31,35] in $Na_2Li_2Ti_6O_{14}$. In addition, there is a broad peak with

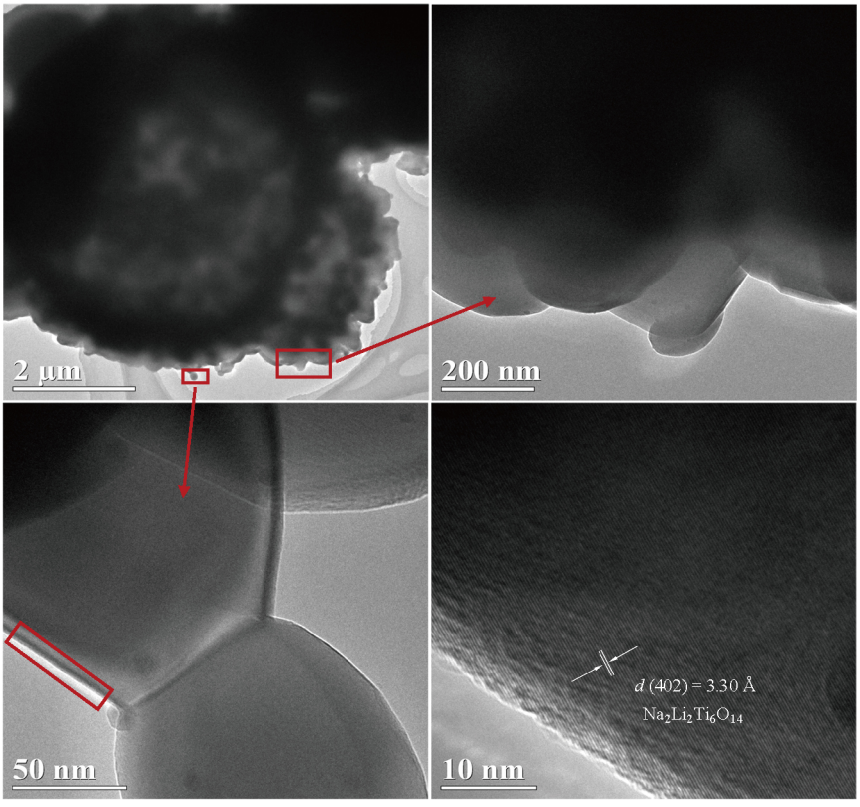

Figure 4 HRTEM images of NLTO-800 sample.

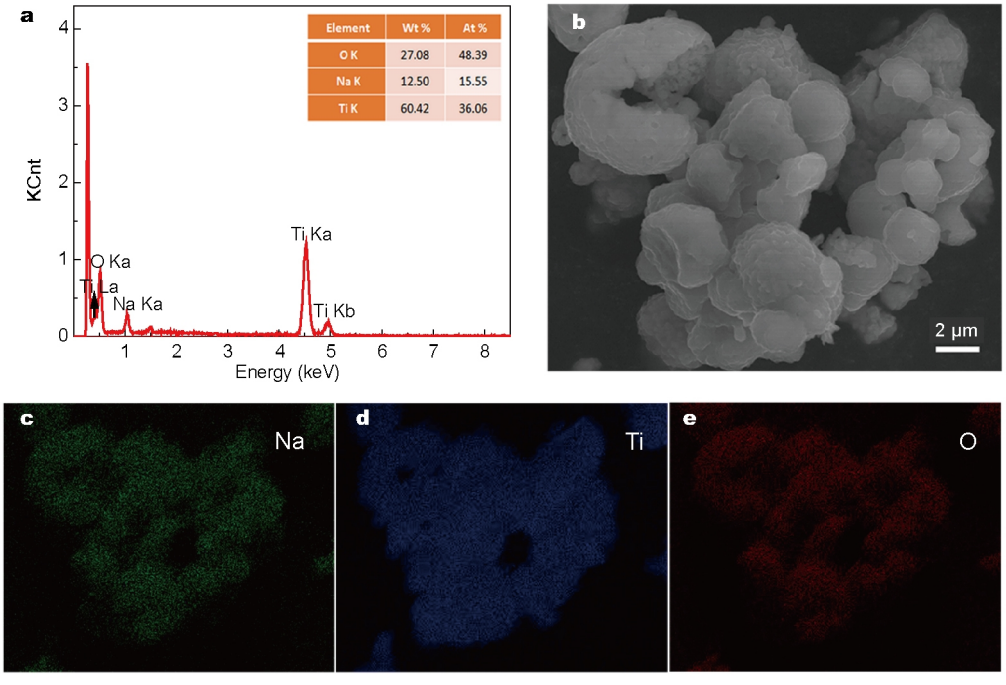

Figure 5 (a, b) EDS images and mapping for (c) Na, (d) Ti, and (e) O elements in NLTO-800 sample.

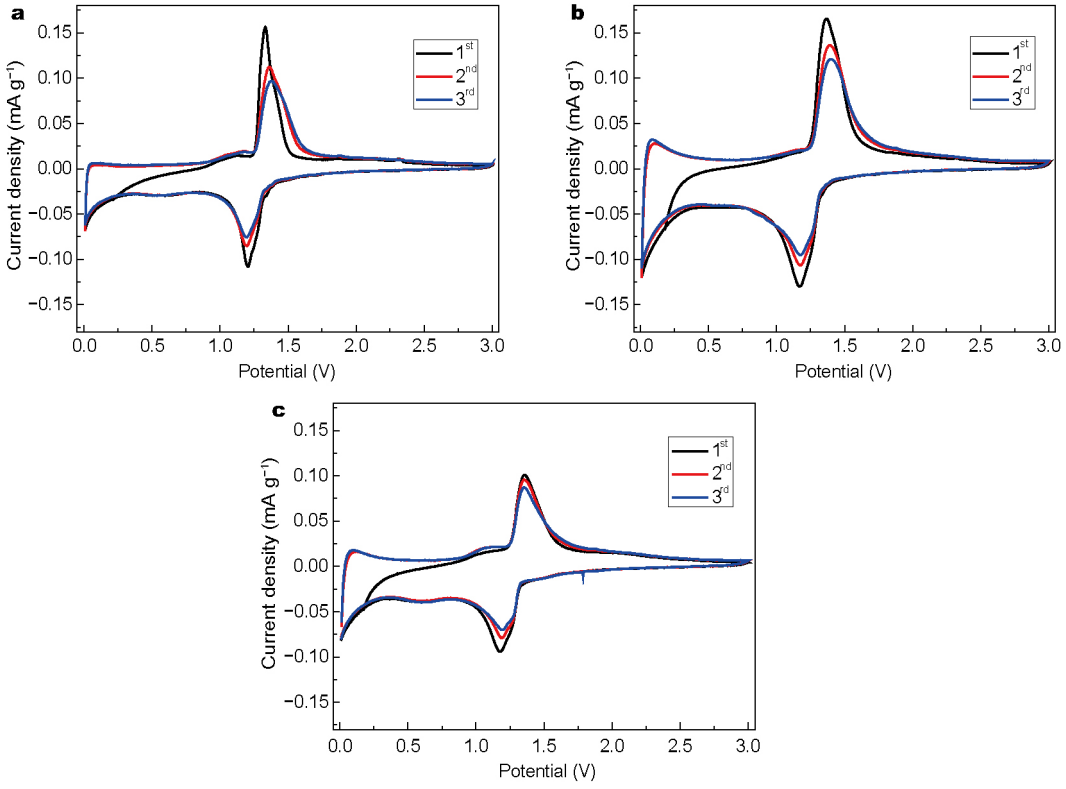

Figure 6 CVs for (a) NLTO-700, (b) NLTO-800 and (c) NLTO-bulk samples.

envelope feature at lower potentials after the second cycles, revealing the formation of amorphous phase when discharging down to 0.1 V. Similar electrochemical behavior can be found in other Ti-based anodes, such as $Li_4Ti_5O_{12}$ and $Li_5Cr_7Ti_6O_{25}$ [36,37]. Furthermore, a cross point between the cathodic and anodic scan was found for the first cycle. The origin for this abnormality may be very complex. Besides the formation of amorphous phase, the inadequate infiltration between the electrolyte and the electrode or the activation of the electrodes may also reduce the current densities of the cathodic scan at low potential, leading to the observed crossover behavior.

Furthermore, the oxidation peak currents of the second CVs are 0.112, 0.137 and 0.095 mA g^{-1} for NLTO-700, NLTO-800 and NLTO-bulk, while the reduction peak currents are 0.083, 0.107 and 0.079 mA g^{-1}, respectively. It was reported that increasing calcination temperature from 800 to 900°C would lead to a much lower peak current due to the aggregation of the $Na_2Li_2Ti_6O_{14}$ particles [31]. However, our results show that the materials calcined at 700 and 900°C are neither well-crystalline nor a pure phase, which in turn results in a relative poor electrochemical performance. In comparison to the NLTO-bulk sample, the peak current of NLTO-800 sample is nearly 1.5 times as much as that of the NLTO-bulk one. As a result, the obtained well-crystalline and hollow hierarchical structure does exhibit a much improved electrochemical performance and a much higher energy density. Furthermore, because the CV curves of the subsequent two cycles are very similar, lithium insertion/extraction to/from the NLTO-800 sample is thus highly reversible.

Fig. 7 shows the charge/discharge profiles, cyclic performances, and Coulombic efficiencies for NLTO-700, NLTO-800 and NLTO-bulk samples at a constant current density of 50 mA g^{-1} between 0.0 and 3.0 V. The charge-discharge potential profiles at 1st, 10th, 30th and 50th cycles for NLTO-700, NLTO-800 and NLTO-bulk samples are presented and compared. The first charge-discharge specific capacities are 171.9/324.9, 203.5/413.8 and 140/260.1 mA h g^{-1} for NLTO-700, NLTO-800 and NLTO-bulk, respectively. It shows that $Na_2Li_2Ti_6O_{14}$ calcined at 800°C has the highest initial charge-discharge capacities. In addition, all anodes show a high irreversible capacity loss, and this phenomenon may be attributed mainly to the side reactions, such as the formation of solid electrolyte interface (SEI), lithium adsorption in the conductive additive carbon black, and irreversible electrochemical decomposition of the electrolyte [38,39]. After 10 cycles, the reversible charge cap-

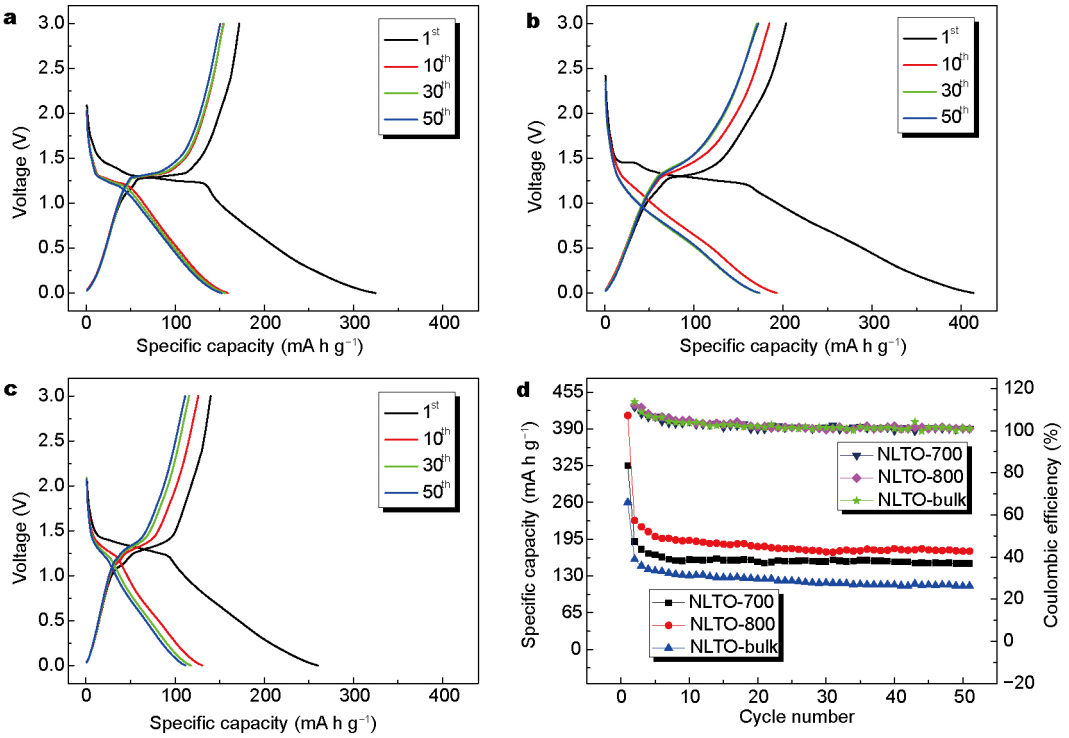

Figure 7 Charge-discharge curves at the 1st, 10th, 30th and 50th cycles for (a) NLTO-700, (b) NLTO-800, and (c) NLTO-bulk samples. (d) Cyclic performance and Coulombic efficiency (at 50 mA g^{-1}) for different samples.

acities are 154, 184.7 and 126.1 mA h g^{-1} for NLTO-700, NLTO-800 and NLTO-bulk, respectively. Owing to the highly reversible lithiation/delithiation behavior in $Na_2Li_2Ti_6O_{14}$ structure, the capacity retention of these three samples is higher than 90%. After 50 cycles, NLTO-800 sample still retains a very high reversible charge capacity (172.3 mA h g^{-1}). In contrast, only 150.6 and 111.4 mA h g^{-1} can be delivered by NLTO-700 and NLTO-bulk, respectively. Besides the specific capacity, NLTO-800 sample also displays the highest Coulombic efficiency. According to the XRD Rietveld refinement, $Na_2Li_2Ti_6O_{14}$ calcined at 800°C shows a larger lattice constant than those calcined at 600 and 700°C. The expanded channels will facilitate the diffusion of lithium ions within the materials, leading to the improved electrochemical performance. The poor cycling stability of NLTO-700 and NLTO-bulk with respect to NLTO-800 is either related to the poor crystalline degree or the absence of well-controlled morphology. It can be concluded that the $Na_2Li_2Ti_6O_{14}$ obtained at 800°C exhibits the highest reversible capacity and a much slower capacity fade, which is very crucial for the materials acting as anode for lithium-ion battery applications.

Furthermore, it should be noted that the voltage plateau of NLTO-800 will gradually disappear during cycling. Such an electrochemical behavior can also be found in other Ti-based anodes, and the study on $Li_4Ti_5O_{12}$ at low voltage range also confirms the gradual loss of the 1.5 V plateau [40]. According to the CV curves, it can be identified that for NLTO-800, there is a bigger and broader peak with envelope feature at low potentials than NLTO-bulk and NLTO-700. This indicates that NLTO-800 is more inclined to generate amorphous phase when discharging down to 0.0 V than NLTO-bulk and NLTO-700, which is responsible for the gradual loss of the 1.3 V plateau for NLTO-800.

The rate performances of the samples and the corresponding charge-discharge curves are depicted in Fig. 8. The rate capabilities were recorded at different rates ranging from 50 to 2800 mA g^{-1} for every 10 cycles. For a large discharging rate, the charging rate is set to be 50 mA g^{-1}. It can be seen that only one voltage platform around 1.25 V is found in Fig. 8a–c, which is in accordance with the feature redox peaks of the CV curves (Fig. 6). Even if it was discharged down to the 0 V, all $Na_2Li_2Ti_6O_{14}$ samples still maintain their high structural integrity and cyclic reversibility. It can be found that NLTO-bulk can deliver a reversible capacity of 187 (50 mA g^{-1}), 125.3 (140 mA g^{-1}), 108.3 (280 mA g^{-1}), 88.7 (560 mA g^{-1}), 69.2 (1400 mA g^{-1}), 54.8 mA h g^{-1} (2800 mA g^{-1}) at different rates. When the structure and morphology are changed, the reversible cap-

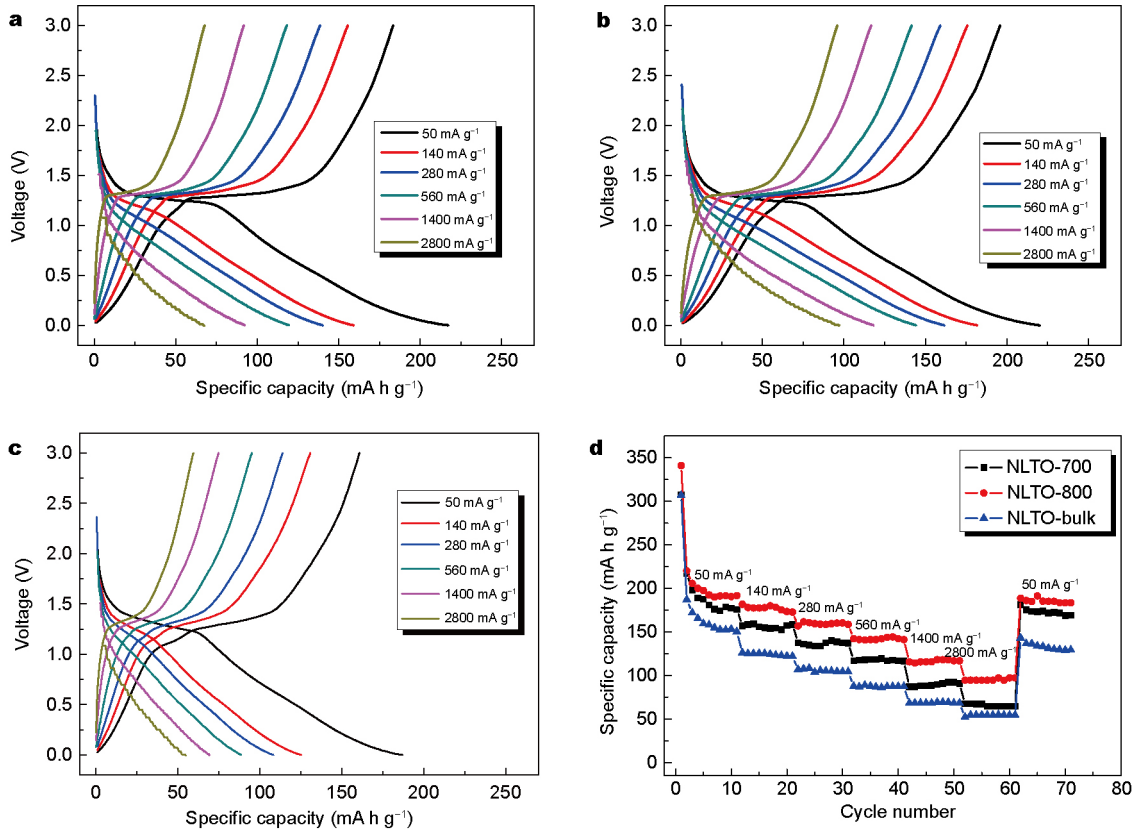

Figure 8 Charge-discharge curves for (a) NLTO-700, (b) NLTO-800 and (c) NLTO-bulk samples and (d) rate capabilities for NLTO-700, NLTO-800 and NLTO-bulk.

acity will be affected as well. For NLTO-700, the reversible capacity was enhanced at any charge-discharge rates and the values are 217.1 (50 mA g^{-1}), 159.1 (140 mA g^{-1}), 140.1 (280 mA g^{-1}), 119.4 (560 mA g^{-1}), 92.2 (1400 mA g^{-1}) and 67.4 mA h g^{-1} (2800 mA g^{-1}). Such an enhancement of the electrochemical performance is related to the hollow and hierarchical morphology, which is very helpful for reducing the charge transfer resistance and for significantly increasing ionic and electronic conductivity. For the material calcined at 800°C, its reversible capacity and rate capability are even much better because of the well-crystallization. After a series of repeated cycles under different rates, when the condition was reset to 50 mA g^{-1}, the discharge capacities of the NLTO-700, NLTO-800 and NLTO-bulk cathodes are recovered to 175.3, 188.7 and 136.5 mA h g^{-1}. The capacity retention rates of the three samples are 80.7%, 85.7% and 72.9% of initial values, respectively. Although the discharge capacities of all the three samples decrease with increasing rates due to the polarization, it is no doubt that the rate capability of NLTO-800 is indeed much better than that of NLTO-700 and NLTO-bulk.

To quantitatively determine the diffusion dynamics, the EIS measurement was performed. The EIS patterns for NLTO-700, NLTO-800 and NLTO-bulk samples are shown in Fig. 9. The spectra contains a depressed semicircle in the high frequency region, which is related to the charge transfer resistance (R_{ct}) for lithium ions reacting at the electrolyte and electrode interface, and a straight line in the low frequency region, which is correlated to the chemical diffusion of lithium ions. Our numerical data suggest that the charge transfer resistance for NLTO-800 is much lower than those for NLTO-700 and NLTO-bulk. Small charge transfer resistance is beneficial for the reversible extraction and insertion of lithium ion during charge and discharge processes, leading to a good cycling performance. Our results confirm that NLTO-800 has the highest electrochemical performance during cycling.

Furthermore, relying on Fig. 9, the diffusion coefficient of lithium ions (D_{Li}) can also be calculated. The equation for calculating D_{Li} can be expressed as [41,42],

$$Z_{re} = R_{ct} + R_s + \sigma\omega^{-\frac{1}{2}}, \quad (1)$$

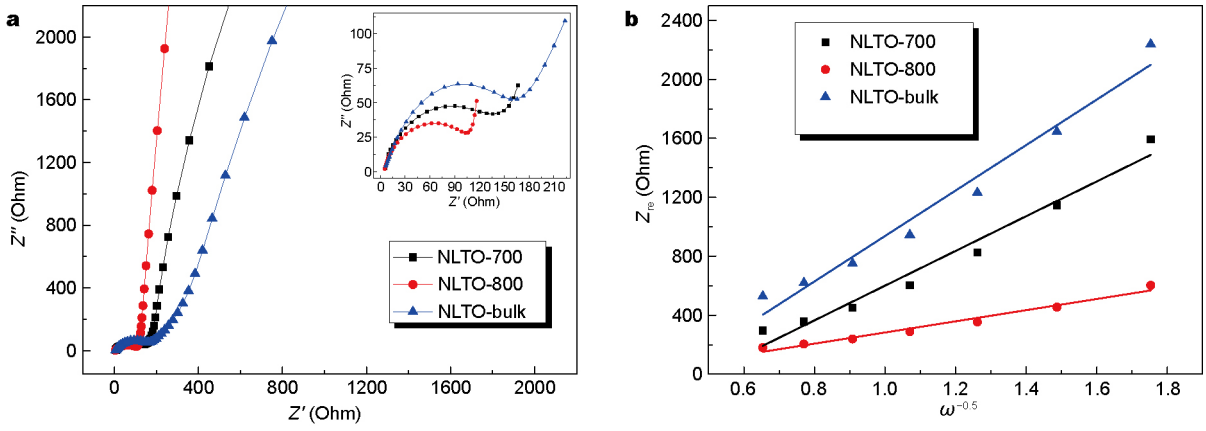

Figure 9 (a) Nyquist plot and (b) Z_{re} as a function of $\omega^{-0.5}$ at low-frequency region for NLTO-700, NLTO-800 and NLTO-bulk samples.

$$D_{Li} = \frac{2R^2T^2}{A^2n^4F^4C_{Li}^2\sigma^2}, \quad (2)$$

where R, T, A, n, F, C_{Li} are the gas constant, the absolute temperature, the surface area of the positive-electrode, the number of electrons transferred in the half-reaction for the redox couple, the Faraday constant, and the concentration of lithium ion in solid, respectively, while σ denotes as the Warburg factor. As reported, the relationship between the real part of impedance (Z_{re}) and σ_w is governed by Equation (1) [43]. Z_{re} as a function of the reciprocal root square of the lower angular frequencies ($\omega^{-0.5}$) is displayed in Fig. 9b, and the calculated data are summarized in Table 2.

It is clear that the NLTO-800 sample possesses the high lithium ion diffusion coefficient (5.33×10^{-16} cm^2 s^{-1}), while NLTO-700 and NLTO-bulk samples reveal a low lithium ion diffusion coefficient (5.51×10^{-17} and 4.75×10^{-17} cm^2 s^{-1}). The results again confirm that NLTO-800 does have a better diffusion kinetic with respect to other samples.

Table 2 EIS for different $Na_2Li_2Ti_6O_{14}$ samples

Samples	NLTO-700	NLTO-800	NLTO-bulk
σ (Ω s$^{-0.5}$)	1,177.62	378.51	896.52
D_{Li} (cm^2 s^{-1})	5.51×10^{-17}	5.33×10^{-16}	3.21×10^{-17}

CONCLUSION

Hollow spherical $Na_2Li_2Ti_6O_{14}$ was successfully synthesized by a solvent thermal process. The micro spherical $Na_2Li_2Ti_6O_{14}$ samples have a much better electrochemical performance than that of bulk one due to the favorable hollow and hierarchal spheres composed of a series of nanoparticles. Especially, $Na_2Li_2Ti_6O_{14}$ formed at 800°C shows a lower charge-transfer resistance, a higher redox activity, and a larger lithium ion diffusion coefficient than the sample prepared at 700°C and the bulk one, which results in the best electrochemical performance among all samples. $Na_2Li_2Ti_6O_{14}$ formed at 800°C can deliver a reversible capacity of 181.7 mA h g^{-1} at 140 mA g^{-1} and 97.2 mA h g^{-1} at 2800 mA g^{-1}. In contrast, the reversible capacity for $Na_2Li_2Ti_6O_{14}$ obtained at 700°C is only 159.1 mA h g^{-1} at 140 mA g^{-1} and 67.4 mA h g^{-1} at 2800 mA g^{-1}. These results indicate that the suitable preparation temperature of $Na_2Li_2Ti_6O_{14}$ is 800°C by the solvent thermal reaction route. The material is expected to be a promising anode material for lithium ion batteries due to its good rate performance and lower cost.

Received 4 January 2017; accepted 10 April 2017; published online 26 April 2017

1 Massé RC, Uchaker E, Cao G. Beyond Li-ion: electrode materials for sodium- and magnesium-ion batteries. Sci China Mater, 2015, 58: 715–766
2 Pan L, Zhu XD, Xie XM, *et al.* Smart hybridization of TiO_2 nanorods and Fe_3O_4 nanoparticles with pristine graphene nanosheets: hierarchically nanoengineered ternary heterostructures for high-rate lithium storage. Adv Funct Mater, 2015, 25: 3341–3350
3 Xu H, Zhu XD, Sun KN, *et al.* Elaborately designed hierarchical heterostructures consisting of carbon-coated TiO_2(B) nanosheets decorated with Fe_3O_4 nanoparticles for remarkable synergy in high-rate lithium storage. Adv Mater Interfaces, 2015, 2: 1500239
4 Pan L, Zhu XD, Xie XM, *et al.* Delicate ternary heterostructures achieved by hierarchical co-assembly of Ag and Fe_3O_4 nanoparticles on MoS_2 nanosheets: morphological and compositional synergy in reversible lithium storage. J Mater Chem A, 2015, 3: 2726–2733
5 Shen L, Yuan C, Luo H, *et al.* Facile synthesis of hierarchically porous $Li_4Ti_5O_{12}$ microspheres for high rate lithium ion batteries. J Mater Chem, 2010, 20: 6998–7004
6 Li W, Zeng L, Wu Y, *et al.* Nanostructured electrode materials for lithium-ion and sodium-ion batteries *via* electrospinning. Sci

China Mater, 2016, 59: 287–321
7 Wang W, Wang H, Wang S, *et al.* Ru-doped $Li_4Ti_5O_{12}$ anode materials for high rate lithium-ion batteries. J Power Sources, 2013, 228: 244–249
8 Lin X, Qian S, Yu H, *et al.* Advanced $BaLi_2Ti_6O_{14}$ anode fabricated *via* lithium site substitution by magnesium. ACS Sustain Chem Eng, 2016, 4: 4859–4867
9 Dambournet D, Belharouak I, Ma J, *et al.* Template-assisted synthesis of high packing density $SrLi_2Ti_6O_{14}$ for use as anode in 2.7-V lithium-ion battery. J Power Sources, 2011, 196: 2871–2874
10 Yin SY, Song L, Wang XY, *et al.* Reversible lithium storage in $Na_2Li_2Ti_6O_{14}$ as anode for lithium ion batteries. Electrochem Commun, 2009, 11: 1251–1254
11 Dambournet D, Belharouak I, Amine K. $MLi_2Ti_6O_{14}$ (M = Sr, Ba, 2Na) lithium insertion titanate materials: a comparative study. Inorg Chem, 2010, 49: 2822–2826
12 Belharouak I, Amine K. $Li_2MTi_6O_{14}$ (M=Sr, Ba): new anodes for lithium-ion batteries. Electrochem Commun, 2003, 5: 435–438
13 Wu K, Wang D, Lin X, *et al.* Comparative study of $Na_2Li_2Ti_6O_{14}$ prepared by different methods as advanced anode material for lithium-ion batteries. J Electroanal Chem, 2014, 717-718: 10–16
14 Khan MM, Ansari SA, Pradhan D, *et al.* Band gap engineered TiO_2 nanoparticles for visible light induced photoelectrochemical and photocatalytic studies. J Mater Chem A, 2014, 2: 637–644
15 Zhang Z, Zhang L, Hedhili MN, *et al.* Plasmonic gold nanocrystals coupled with photonic crystal seamlessly on TiO_2 nanotube photoelectrodes for efficient visible light photoelectrochemical water splitting. Nano Lett, 2013, 13: 14–20
16 Duan H, Li J, Du H, *et al.* Tailoring native defects and zinc impurities in $Li_4Ti_5O_{12}$: insights from first-principles study. J Phys Chem C, 2015, 119: 5238–5245
17 Ge H, Tian H, Song H, *et al.* Study on the energy band structure and photoelectrochemical performances of spinel $Li_4Ti_5O_{12}$. Mater Res Bull, 2015, 61: 459–462
18 Wu K, Shu J, Lin X, *et al.* Enhanced electrochemical performance of sodium lithium titanate by coating various carbons. J Power Sources, 2014, 272: 283–290
19 Lao M, Li P, Lin X, *et al.* Enhanced lithium storage property of Na-doped $Li_2Na_2Ti_6O_{14}$ anode materials for secondary lithium-ion batteries. RSC Adv, 2015, 5: 41999–42008
20 Qian S, Yu H, Yan L, *et al.* Ag enhanced electrochemical performance for $Na_2Li_2Ti_6O_{14}$ anode in rechargeable lithium-ion batteries. Ceramics Int, 2016, 42: 6874–6882
21 Wang P, Qian S, Yi TF, *et al.* Effect of sodium-site doping on enhancing the lithium storage performance of sodium lithium titanate. ACS Appl Mater Interfaces, 2016, 8: 10302–10314
22 Liu J, Du C, Tang Z, *et al.* *In situ* nickel/carbon coated lithium titanium oxide anode material with improved electrochemical properties. Electrochim Acta, 2014, 143: 56–62
23 Wu K, Lin X, Shao L, *et al.* Copper/carbon coated lithium sodium titanate as advanced anode material for lithium-ion batteries. J Power Sources, 2014, 259: 177–182
24 He N, Wang B, Huang J. Preparation and electrochemical performance of monodisperse $Li_4Ti_5O_{12}$ hollow spheres. J Solid State Electrochem, 2010, 14: 1241–1246
25 Wang L, Hu Z, Zhao K, *et al.* Hollow spherical $LiNi_{0.5}Mn_{1.5}O_4$ built from polyhedra with high-rate performance via carbon nanotube modification. Sci China Mater, 2016, 59: 95–103
26 Ding YL, Zhao XB, Xie J, *et al.* Double-shelled hollow microspheres of $LiMn_2O_4$ for high-performance lithium ion batteries. J Mater Chem, 2011, 21: 9475–9479
27 Shi SJ, Lou ZR, Xia TF, *et al.* Hollow $Li_{1.2}Mn_{0.5}Co_{0.25}Ni_{0.05}O_2$ microcube prepared by binary template as a cathode material for lithium ion batteries. J Power Sources, 2014, 257: 198–204
28 Chou SL, Wang JZ, Liu HK, *et al.* Rapid synthesis of $Li_4Ti_5O_{12}$ microspheres as anode materials and its binder effect for lithium-ion battery. J Phys Chem C, 2011, 115: 16220–16227
29 Tang Y, Yang L, Fang S, *et al.* $Li_4Ti_5O_{12}$ hollow microspheres assembled by nanosheets as an anode material for high-rate lithium ion batteries. Electrochim Acta, 2009, 54: 6244–6249
30 Li J, Cao C, Xu X, *et al.* $LiNi_{1/3}Co_{1/3}Mn_{1/3}O_2$ hollow nano-micro hierarchical microspheres with enhanced performances as cathodes for lithium-ion batteries. J Mater Chem A, 2013, 1: 11848–11852
31 Shu J, Wu K, Wang P, *et al.* Lithiation and delithiation behavior of sodium lithium titanate anode. Electrochim Acta, 2015, 173: 595–606
32 Wang P, Li P, Yi TF, *et al.* Improved lithium storage performance of lithium sodium titanate anode by titanium site substitution with aluminum. J Power Sources, 2015, 293: 33–41
33 Wu K, Shu J, Lin X, *et al.* Phase composition and electrochemical performance of sodium lithium titanates as anode materials for lithium rechargeable batteries. J Power Sources, 2015, 275: 419–428
34 Yang X, Wang X, Zou G, *et al.* Spherical lithium-rich layered $Li_{1.13}[Mn_{0.534}Ni_{0.233}Co_{0.233}]_{0.87}O_2$ with concentration-gradient outer layer as high-performance cathodes for lithium ion batteries. J Power Sources, 2013, 232: 338–347
35 Yin SY, Feng CQ, Wu SJ, *et al.* Molten salt synthesis of sodium lithium titanium oxide anode material for lithium ion batteries. J Alloys Compd, 2015, 642: 1–6
36 Yi TF, Mei J, Zhu YR, *et al.* $Li_5Cr_7Ti_6O_{25}$ as a novel negative electrode material for lithium-ion batteries. Chem Commun, 2015, 51: 14050–14053
37 Yi TF, Xie Y, Zhu YR, *et al.* Structural and thermodynamic stability of $Li_4Ti_5O_{12}$ anode material for lithium-ion battery. J Power Sources, 2013, 222: 448–454
38 Lan H, Qian S, Wang Q, *et al.* $Sr_{1-x}Na_{2x}Li_2Ti_6O_{14}$ ($0\leq x\leq 1$) as anode materials for rechargeable Li-ion batteries. Ceramics Int, 2017, 43: 1552–1557
39 Borghols WJH, Wagemaker M, Lafont U, *et al.* Size effects in the $Li_{4+x}Ti_5O_{12}$ spinel. J Am Chem Soc, 2009, 131: 17786–17792
40 Yi TF, Shu J, Zhu YR, *et al.* High-performance $Li_4Ti_{5-x}V_xO_{12}$ ($0\leq x\leq 0.3$) as an anode material for secondary lithium-ion battery. Electrochim Acta, 2009, 54: 7464–7470
41 Yang SY, Yuan J, Zhu YR, *et al.* Structure and electrochemical properties of Sc^{3+}-doped $Li_4Ti_5O_{12}$ as anode materials for lithium-ion battery. Ceramics Int, 2015, 41: 7073–7079
42 Yi TF, Han X, Yang SY, *et al.* Enhanced electrochemical performance of Li-rich low-Co $Li_{1.2}Mn_{0.56}Ni_{0.16}Co_{0.08-x}Al_xO_2$ ($0\leq x\leq 0.08$) as cathode materials. Sci China Mater, 2016, 59: 618–628
43 Hu YS, Kienle L, Guo YG, *et al.* High lithium electroactivity of nanometer-sized rutile TiO_2. Adv Mater, 2006, 18: 1421–1426

Acknowledgments This work was supported by the National Natural Science Foundation of China (21301052 and 51404002), Natural Science Foundation of Heilongjiang Province (E2016056), Specialized Research Fund for the Doctoral Program of Higher Education (20132301120001), Postdoctoral Science-Research Developmental Foundation of Heilongjiang Province (LBH-Q13138), and Applied Technology Research and Development Program of Harbin (2015RAQXJ032).

Author contributions Xie Y and Zhu YR conceived the strategy and supervised the design of experiments. Fan SS, Zhong H and Lou M performed the experiments on the materials synthesis, characterization, and electrochemical measurements. Fan SS wrote the manuscript, and all authors participated in the revision of the manuscript. Yu HT was involved in data analysis and discussion.

Conflict of interest The authors declare that they have no conflict of interest.

Supplementary information Supporting data are available in the online version of the paper.

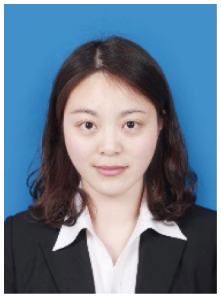

Shan-Shan Fan received her BSc degree in applied chemistry from Luoyang Normal University in 2015. She entered Heilongjiang University to pursue her master's degree in science in 2015. She is interested in the application of quantum chemistry and the synthesis and electrochemical performance of anode materials for lithium ion battery applications.

Ying Xie received his BE degree in fine chemical engineering from Harbin University of Science and Technology in 2002. He then obtained MSc degree in chemical engineering in 2004 and PhD degree in chemical engineering and technology from Harbin Institute of Technology in 2008. He joined Heilongjiang University in 2008, and then became a member of the Key Laboratory of Functional Inorganic Material Chemistry. He is currently a professor of Heilongjiang University. His research interests include theoretical predictions on the structures and properties of inorganic compounds and the synthesis of electrode materials and their applications in lithium-ion battery.

具有中空分级结构的$Na_2Li_2Ti_6O_{14}$微球作为高性能锂离子电池负极材料

范姗姗[1], 仲华[1], 于海涛[1], 娄明[1], 谢颖[1*], 朱彦荣[2*]

摘要 本文采用溶剂热法合成了球形$Na_2Li_2Ti_6O_{14}$材料. 所有溶剂热法制备得到的材料均具有中空的分级结构, 并且均由粒径约为300 nm的初级粒子通过组装形成, 微球的直径大约为2−3 μm. 粒子的形貌分析表明, 随着合成温度的增加, 孔隙率逐渐增加且中空结构更加明显. 在所有材料中, 800°C合成的$Na_2Li_2Ti_6O_{14}$具有最好的电化学性能. 充放电测试表明, 在电流密度为50、140、280、560、1400、2800 mA g^{-1}时, 800°C合成的$Na_2Li_2Ti_6O_{14}$样品的可逆容量分别为220.1、181.7、161.6、144.2、118.1、97.2 mA h g^{-1}. 但是在相同电流密度条件下, 块状的$Na_2Li_2Ti_6O_{14}$的可逆容量分别为187、125.3、108.3、88.7、69.2、54.8 mA h g^{-1}. 中空分级结构微球可以有效地减小锂离子的扩散距离、增加电极与电解液的接触面积、以及缓冲锂离子嵌脱过程中的体积变化, 从而使其具有较高的电化学性能.